Effects of Ice Clouds on Barotropic and Baroclinic Processes during TOGA COARE

Guoqing Zhai and Xiaofan Li

School of Earth Sciences, Zhejiang University, Hangzhou, Zhejiang, China

Summary

Effects of ice clouds on barotropic and baroclinic processes over the deep tropical convective regime are examined through the analysis of difference in budget of perturbation kinetic energy between the control and sensitivity two-dimensional cloud-resolving model simulations. The sensitivity experiment excludes ice hydrometeor and associated microphysical processes. Both experiments are imposed by large-scale forcing from Tropical Ocean Global Atmosphere (TOGA) Coupled Ocean Atmosphere Response Experiment (COARE) (Fig. 1). The exclusion of ice clouds generally enhances baroclinic conversion from perturbation available potential energy and reduces barotropic conversion from perturbation kinetic energy to mean kinetic energy (Figs. 2 and 3). The analysis of the root-mean-squared difference and linear correlation coefficient using data of difference budget between sensitivity and control experiments reveals that while baroclinic conversion process plays a major role in budget difference, barotropic conversion processes show a significant modification in the tendency difference in perturbation circulations (Fig. 4). While both experiments are imposed by the same large-scale forcing, the difference in barotropic conversion between the two experiments is associated with the difference in vertical flux of zonal momentum (Fig. 5). The differences in vertical flux of zonal momentum and barotroic conversion are positively correlated near the surface whereas they are negatively correlated in the mid and upper troposphere (Fig. 6). The differences in tendency of vertical flux of zonal momentum and zonal flux of ice hydrometeor have the smallest root-mean-squared difference, indicating that the difference in zonal flux of ice hydrometeor accounts for the difference in tendency of vertical flux of zonal momentum (Fig. 7).

Perturbation kinetic-energy budget

$$\frac{\partial K'}{\partial t} = C_u(\overline{K}, K') + C_w(\overline{K}, K') + C(P', K') + G_{qv}(K') + G_{ql}(P')$$

$$K' = [\frac{\overline{(u')^2 + (w')^2}}{2}]$$

$$C_u(\overline{K}, K') = -[\overline{u'w'}\frac{\partial \overline{u}^o}{\partial z}]$$

$$C_w(\overline{K}, K') = -[\overline{w'w'}\frac{\partial \overline{w}^o}{\partial z}]$$

$$C(P', K') = [g\frac{\overline{w'T'}}{T_b}]$$

$$G_{qv}(K') = [0.61 g \overline{w' q_v'}]$$

$$G_{ql}(K') = -[g \overline{w' q_l'}]$$

$$[()] = \int_{z_b}^{z_t} \overline{\rho}()dz$$

$$BKEC = BKEC1 * \mathrm{BKEC2}$$

$$\mathrm{BKEC1} = d\overline{u}^o$$

$$BKEC2 = -\overline{\rho}\,\overline{u'w'}$$

Budget of vertical flux of zonal momentum

$$BKEC2_t = BKEC2_d + BKEC2_p + BKEC2_{b1} + BKEC_{b2} + BKEC_{b3}$$

$$BKEC2_t = \frac{\partial}{\partial t} BKEC2 = \frac{\partial}{\partial t}(-\overline{\rho}\,\overline{u'w'})$$

$$BKEC2_d = \overline{\overline{\rho} w' \frac{\partial}{\partial x}(2u'\overline{u}^o + u'u')} + \overline{w'\frac{\partial}{\partial z}\overline{\rho}(w'\overline{u}^o + \overline{w}^o u' + w'u')}$$

$$+ \overline{\overline{\rho} u' \frac{\partial}{\partial x}(u'\overline{w}^o + \overline{u}^o w' + u'w')} + \overline{u'\frac{\partial}{\partial z}\overline{\rho}(2w'\overline{w}^o + w'w')}$$

$$BKEC2_p = c_p \overline{\rho}\, \overline{w'\frac{\partial(\overline{\theta}\pi')}{\partial x} + u'\frac{\partial(\overline{\theta}\pi')}{\partial z}}$$

$$BKEC2_{b1} = -\overline{\rho} g \overline{u'\frac{\theta'}{\theta_o}}$$

$$BKEC2_{b2} = -0.61\overline{\rho} g \overline{u'q_v'}$$

$$BKEC2_{b3} = \overline{\rho} g \overline{u'q_l'}$$

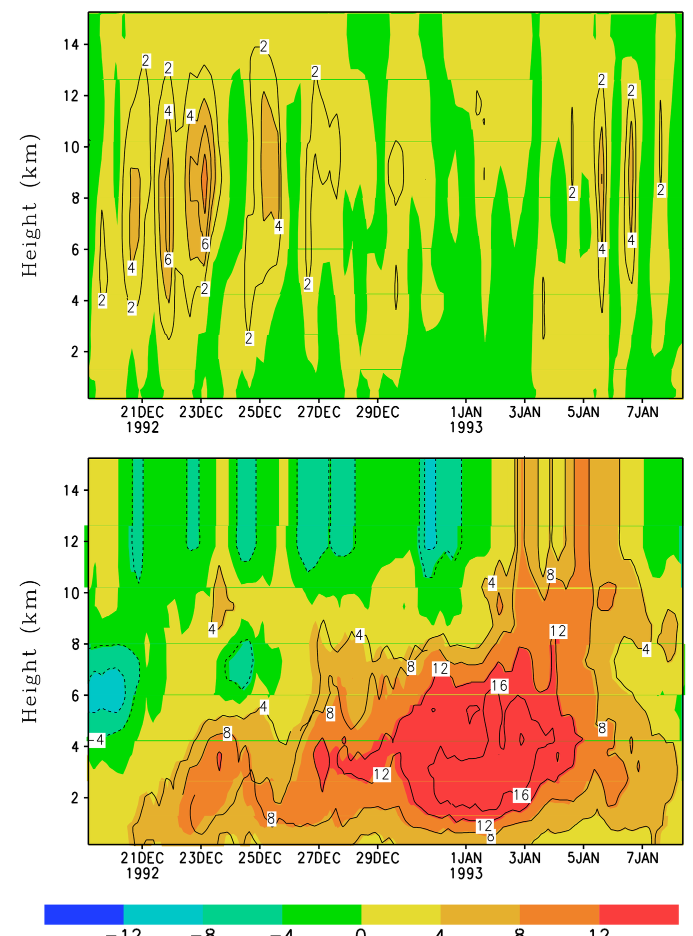

Fig. 1 Temporal and vertical distribution of large-scale forcing including (a) vertical velocity (cm s^{-1}) and (b) zonal wind (m s^{-1}) from TOGA COARE.

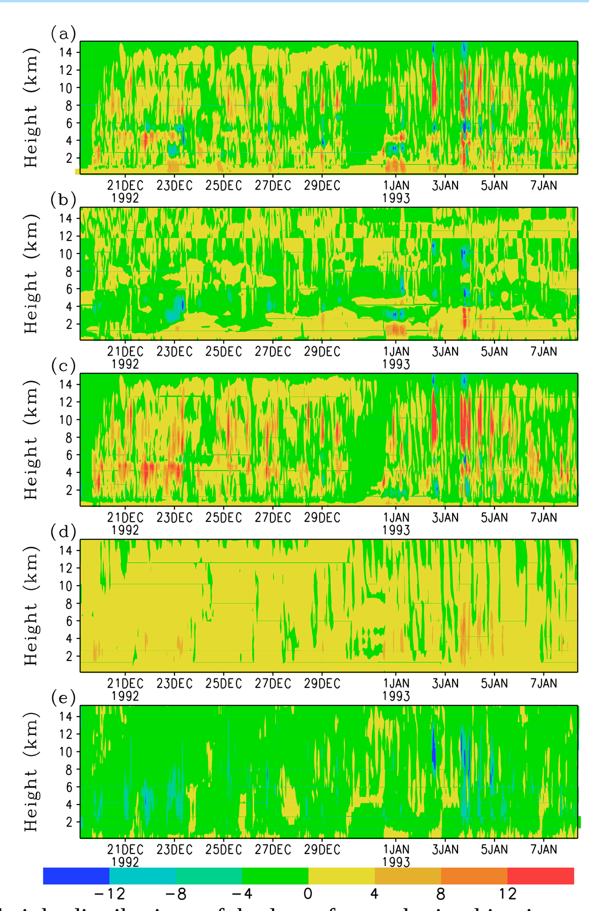

Fig. 2 Time-height distributions of budget of perturbation kinetic energy [(a) tendency of perturbation kinetic energy, (b) barotropic conversion between mean and perturbation kinetic energy and baroclinic conversion between perturbation available potential energy and kinetic energy due to vertical flux of (c) heat, (d) water vapor and (e) cloud hydrometeors] in control experiments.

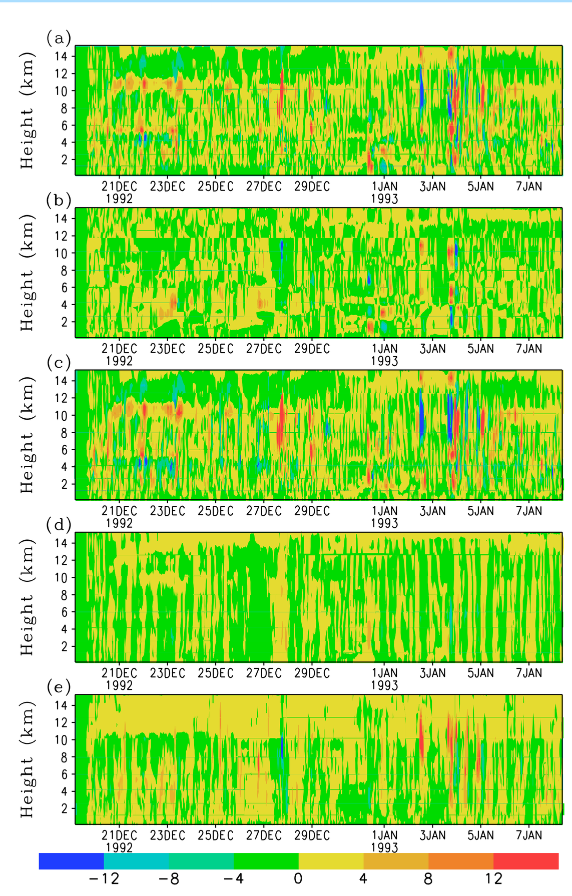

Fig. 3 As in Fig. 2 except for those of differences between sensitivity and control experiments.

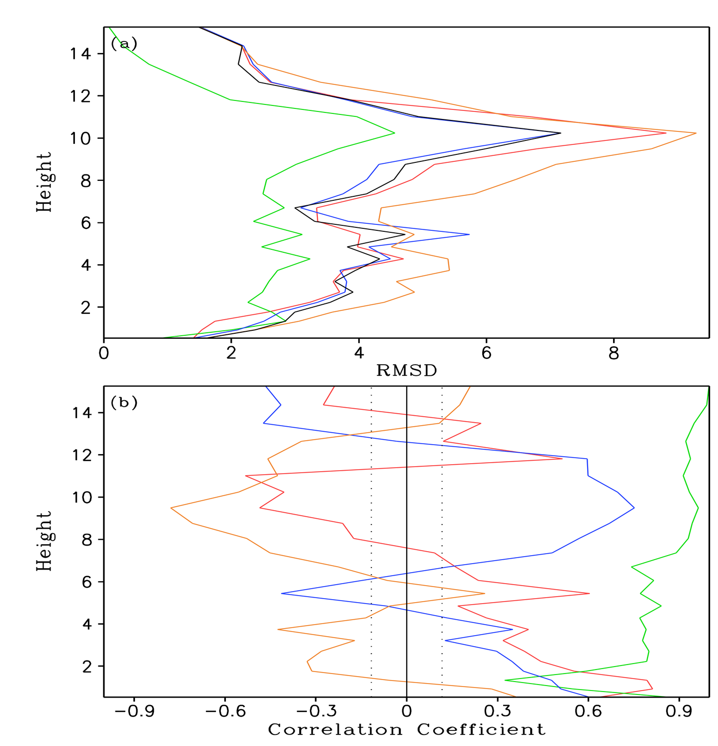

Fig. 4 Vertical profiles of (a) root-mean-squared differences (RMSDs; 10^5 Js^{-1}) and (b) correlation coefficients between tendency of perturbation kinetic energy and barotropic conversion (red), baroclinic conversion between perturbation available potential energy and kinetic energy due to vertical flux of heat (green), water vapor (blue) and cloud hydrometeors (orange)calculated using difference data between sensitivity and control experiments. Black solid line denotes the standard deviation of the tendency in (a), and dotted lines denote critical correlation coefficients for 99% confidence level in (b).

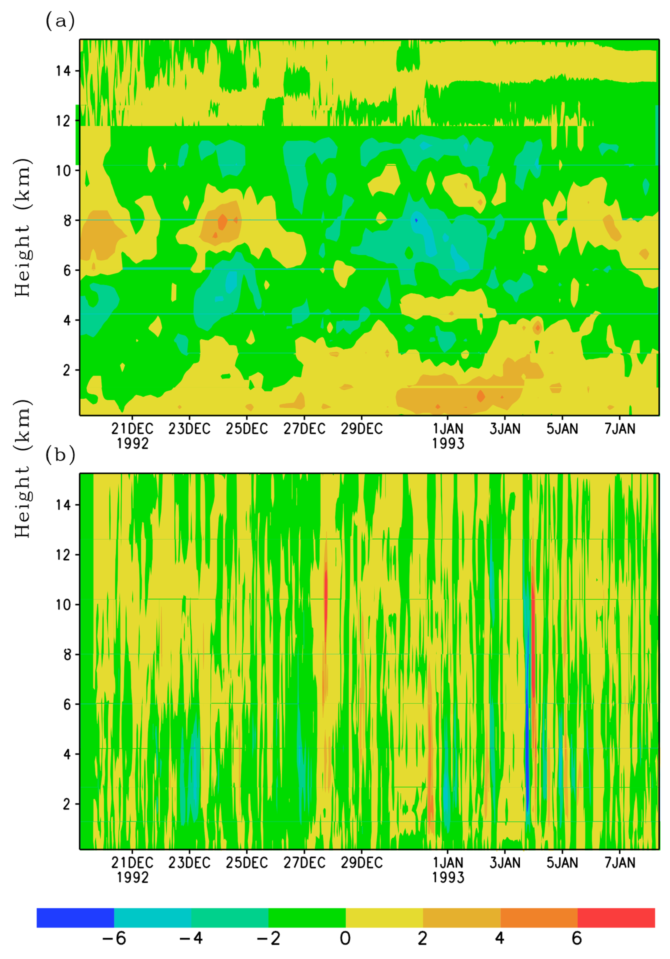

Fig. 5 Time-height distributions of (a) imposed zonal-wind difference in vertical layer (BKEC1; ms^{-1}) and (b) difference in vertical flux of zonal momentum (BKEC2; 10^5 Jm^{-1}) between sensitivity and control experiments.

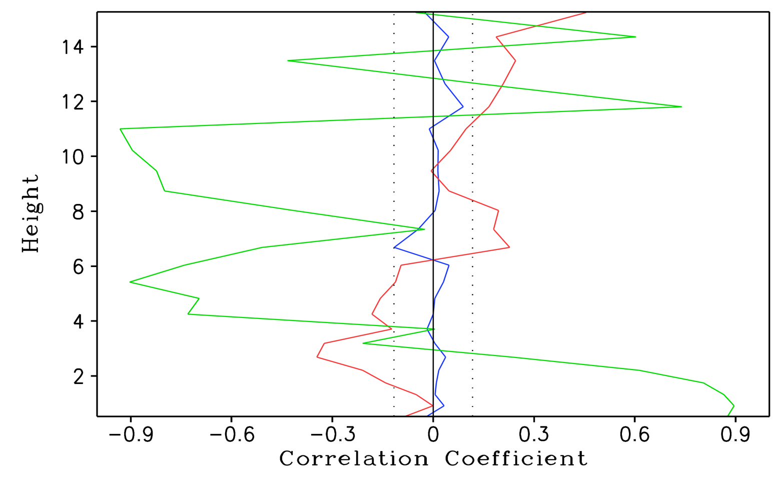

Fig. 6 Vertical profile of correlation coefficient between vertical wind shear and vertical flux of zonal momentum shown in Fig. 4 (blue) and vertical wind shear and barotropic conversion (red) and vertical flux of zonal momentum and barotropic conversion (green). Dotted lines denote critical correlation coefficients for 99% confidence level.

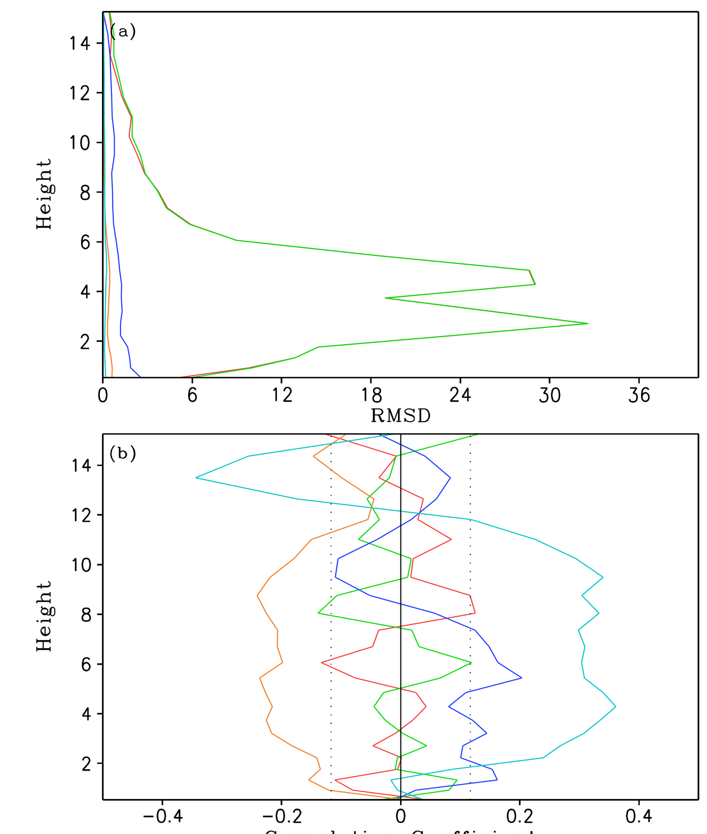

Fig. 7 Vertical profiles of (a) root-mean-squared differences (RMSDs; 10^4 $Jm^{-1}s^{-1}$) and (b) correlation coefficients between Term $BKEC2_t$ and Term $BKEC2_d$ (red), Term $BKEC2_t$ and Term $BKEC2_p$ (green), and Term $BKEC2_t$ and Term $BKEC2_{b1}$ (blue), Term $BKEC2_t$ and Term $BKEC_{b2}$ (orange) and between Term $BKEC2_t$ and Term $BKEC2_{b3}$ (cyan). The standard deviation of Term $BKEC2_t$ is excluded in (a) because it is negligibly small. Dotted lines denote critical correlation coefficients for 99% confidence level in (b).